ACS OMEGA

http://pubs.acs.org/journal/acsodf

Article

Effect of Nanoparticle Weight on the Cellular Uptake and Drug Delivery Potential of PLGA Nanoparticles

Prabhat Kattel,[§] Shoukath Sulthana,[§] Jiří Trousil, Dinesh Shrestha, David Pearson, and Santosh Aryal*

Cite This: *ACS Omega* 2023, 8, 27146−27155

Read Online

ACCESS | Metrics & More | Article Recommendations | Supporting Information

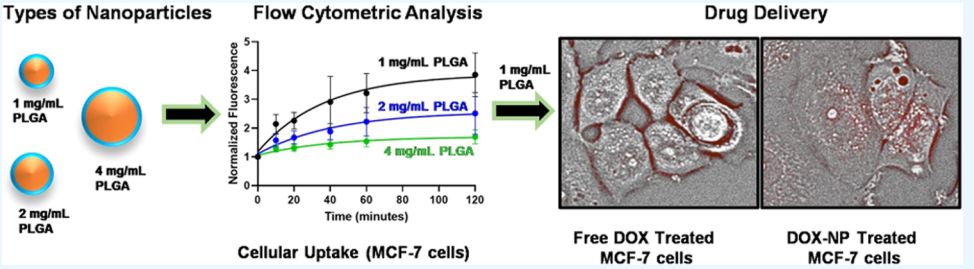

ABSTRACT: Biodegradable and biocompatible polymeric nanoparticles (NPs) stand out as a key tool for improving drug bioavailability, reducing the inherent toxicity, and targeting the intended site. Most importantly, the ease of polymer synthesis and its derivatization to add functional properties makes them potentially ideal to fulfill the requirements for intended therapeutic applications. Among many polymers, US FDA-approved poly(L-lactic-*co*-glycolic) acid (PLGA) is a widely used biocompatible and biodegradable co-polymer in drug delivery and in implantable biomaterials. While many studies have been conducted using PLGA NPs as a drug delivery system, less attention has been given to understanding the effect of NP weight on cellular behaviors such as uptake. Here we discuss the synthesis of PLGA NPs with varying NP weights and their colloidal and biological properties. Following nanoprecipitation, we have synthesized PLGA NP sizes ranging from 60 to 100 nm by varying the initial PLGA feed in the system. These NPs were found to be stable for a prolonged period in colloidal conditions. We further studied cellular uptake and found that these NPs are cytocompatible; however, they are differentially uptaken by cancer and immune cells, which are greatly influenced by NPs' weight. The drug delivery potential of these nanoparticles (NPs) was assessed using doxorubicin (DOX) as a model drug, loaded into the NP core at a concentration of 7.0 ± 0.5 wt % to study its therapeutic effects. The results showed that both concentration and treatment time are crucial factors for exhibiting therapeutic effects, as observed with DOX-NPs exhibiting a higher potency at lower concentrations. The observations revealed that DOX-NPs exhibited a higher cellular uptake of DOX compared to the free-DOX treatment group. This will allow us to reduce the recommended dose to achieve the desired effect, which otherwise required a large dose when treated with free DOX. Considering the significance of PLGA-based nanoparticle drug delivery systems, we anticipate that this study will contribute to the establishment of design considerations and guidelines for the therapeutic applications of nanoparticles.

INTRODUCTION

Organic and inorganic nanoparticles (NPs) have been widely used in the field of nanotheranostics due to their ease of design to target different disease conditions.[1−12] In addition, NPs are increasingly used in consumer products, electronics, and pharmaceuticals. Nowadays, it is impossible to avoid NPs due to their broader environmental existence, for example, the aerial presence of carbon, plastic, and mineral particles, and their existence in many pharmaceutical formulations. These particles interact with our body in many different ways, but their deleterious effects primarily arise from interaction at cellular and subcellular levels.[13] With recent advancements in the chemical synthesis of NPs using bottom-up and top-down methods with various surface chemistries, we have been successful in synthesizing new NPs with unique properties capable of modulating at the nano-bio interface.[9,14−23] Most importantly, biodegradable and biocompatible polymeric NPs stand out as a key tool for improving drug bioavailability, reducing inherent toxicity, and targeting the intended site due to the ease of polymer synthesis and derivatization to add the functional properties required for biological targets.

Among many polymers, US FDA-approved poly(L-lactic-*co*-glycolic) acid (PLGA) is the widely used and most characterized biocompatible and biodegradable co-polymer used to prepare NPs for controlled drug delivery.[24] The drug's

Received: April 4, 2023
Accepted: June 19, 2023
Published: July 19, 2023

association with NPs favorably impacts the pharmacokinetics and biological responses of the drug, as it can be tuned to precisely target the disease sites while minimizing the off-target effects. However, to achieve the aforementioned outstanding outcomes, a safe entry of NPs into the cells is an important step, which is governed by the surface properties of both NPs and cells. For instance, Platel et al.[25] reported the geno- and cytotoxicity of PLGA NPs of varying surface charges: positive, neutral, or negative. The study was conducted in different cell lines such as L5178Y mouse lymphoma cells, TK6 human β-lymphoblastoid cells, and 16HBE14o- human bronchial epithelial cells, which showed high cytotoxicity with positively charged PLGA NPs, whereas negatively charged PLGA NPs were found to be highly biocompatible.[25] A multifunctional PLGA-based anticancer nanomedicine was developed by combining a reductively cleavable surfactant with hyaluronic acid coating, which exhibited a long circulation time, high targetability, and effective inhibition of orthotopic human A549-Luc lung tumor in nude mice.[26] Marasini et al. synthesized cyclic Lyp-1 peptide-functionalized lipid shield PLGA NPs that target the overexpressed p32 receptor in cancer cells.[27] These particles showed differential targeting properties in vitro with maximum particle internalization to cancer cells. These cyclic Lyp-1 functionalized particles were labeled with a near-infrared dye to track in vivo, which showed tumor-targeting efficiency when compared to controlled NPs. A significant accumulation of NPs was found in tumor-bearing NU/NU nude mice.[27] In addition to NPs' cellular and tumor response, PLGA NPs have also been used to design or load contrast agents for imaging purposes. An enhanced magnetic relaxivity has been shown when superparamagnetic iron oxide (SPIO) NPs are clustered into the core of PLGA NPs, which showed great potential in tumor imaging.[28−34] Moreover, several systematic studies evaluating NP cellular uptake have been reported, highlighting the size, chemistry, and shape.[17,35−38] Among these studies, particle size-dependent uptake studies have been widely studied.[36,37] However, the findings from these size-dependent studies have yielded contrasting results, with some research indicating maximum uptake for NPs smaller than 50 nm, while others have highlighted the 100 nm NPs for optimum drug delivery.[22,23,25,39] Therefore, more studies and analytical parameters are needed to develop guidelines that can help in mapping NP cellular uptake.

While efforts have been devoted to the efficacy study of nanodrugs and their reactions in intracellular environments with a focus on size, surface chemical structure, different drug contents, and shape, less attention has been given to the influence of the NP weight that is given by the polymer feeding concentration as well as the resulting NP density. One could hypothesize that the density of nanoparticles (also known as apparent structural density) could affect cellular sequestration.[40] Considering that most of the NP cellular interaction and uptake studies are conducted in two-dimensional in vitro cell culture systems depending on the density gradient distribution and aggregation of NPs in the biological media over time and onto the monolayer of the cell is a crucial step that brings NPs into cellular contact. Therefore, in addition to the size, shape, and surface properties of NPs, the feeding amount of the precipitated polymer and the resulting weight of the interacting NPs are equally important to envision their uptake kinetics. In this report, we focus our research on the synthesis and characterization of PLGA NPs of varying weights to study the cellular uptake and therapeutic potentials against immune and cancer cells in vitro.

MATERIAL AND METHODS

Nanoparticle Preparation. NPs were prepared by the nanoprecipitation method.[22,33,41−44] Briefly, 1,2-distearoyl-*sn*-glycero-3-phosphoethanolamine-*N*-[succinyl-(polyethyleneglycol)-2000] (ammonium salt, DSPE-PEG, #880121, Avanti Polar Lipids, Alabaster, AL) was dissolved in 4% ethanol (260 μg per 2 mL), followed by stirring at 60 °C for 10 min. Subsequently, carboxyl group-terminated PLGA (50:50, inherent viscosity 0.55−0.75 dL/g, #B6013-2, 50 kDa, Birmingham Division, Birmingham, AL) was dissolved in 400 μL of acetonitrile. PLGA with a 50:50 lactic and glycolic acid ratio is reported as a good candidate for sustained drug delivery due to its unified degradation pattern when compared to the PLGA with an increasing lactic acid ratio.[45−47] The rationale behind choosing one type of polymer in this study is to understand the effect of the weight of the NPs, which otherwise is difficult to rationalize while using different molecular-weight polymers. Also, in cellular drug delivery, faster degradation is recommended for dislodging the drug at the target site, as diffusion and degradation-diffusion are the main mechanism of drug release. Three different amounts of PLGA, 1 mg, 2 mg, and 4 mg, were used while keeping the amount of DSPE-PEG constant. For the nanoprecipitation, the acetonitrile solution (400 μL) of PLGA was added dropwise to the DSPE-PEG solution, followed by the addition of 1 mL of cold Milli-Q water to quench the temperature. The mixture was stirred continuously for an additional 1 h, followed by acetonitrile evaporation under reduced pressure (40 °C). By varying the initial amount of PLGA in acetonitrile (1, 2, and 4 mg), NPs with different weight values were prepared and referred to as 1 mg/mL PLGA, 2 mg/mL PLGA, and 4 mg/mL PLGA, respectively.

For the preparation of fluorescent NPs, PLGA stock solutions were supplemented with Nile red (NR, 2 μg of dye per 1 mg of PLGA, #415711000, Thermo Fisher Scientific) or 1,2-dioleoyl-*sn*-glycero-3-phosphoethanolamine-*N*-(lissamine rhodamine B sulfonyl) (ammonium salt) (LissRh, 2 μg of fluorescent lipid per 1 mg of PLGA, #810150, Avanti Polar Lipids) and were used as above.

Nanoparticle Characterization. The size (D_h) and polydispersity index (PDI) of the NPs were measured by dynamic light scattering (DLS) using a Zetasizer Ultra Red (Malvern Panalytical Ltd., Malvern, U.K.). Electrophoretic light scattering (ELS) experiments were carried out using the same instrument. The equipment is also capable of determining the concentration of NPs in a solution, which was measured using the multiangle dynamic light scattering (MADLS) technique. The scattering intensity of water (the dispersant) was measured using backscatter detection. The concentration of all NP types was kept constant at 1 mg/mL for light scattering characterizations. The total dry weight of the NPs was quantified gravimetrically following lyophilization.

Cell Culture. Both human breast cancer MCF-7 cell line (HTB-22) and murine monocyte-macrophages J774A.1 cell line (TIB-67) were obtained from ATCC (American Type Culture Collection, Manassas, VA). Both cell lines were maintained in Dulbecco's Modified Eagle Medium (DMEM, Corning, Corning, NY) supplemented with 10% of heat-inactivated fetal bovine serum (FBS, Corning) and 1% of antibiotic penicillin-streptomycin solution (#SV30010, Hy-

https://doi.org/10.1021/acsomega.3c02273
ACS Omega 2023, 8, 27146−27155

Clone, Logan, UT) in a humidified atmosphere containing 5% CO_2 at 37 °C. In the case of both cell lines, the medium change was performed every 2−3 days and the cells used were between passages 5 and 8.

Cell Compatibility Assay. The cells were seeded in 96-well plates at a density of 10 000 cells per well. The next day, the medium was replaced with a fresh culture medium containing the tested formulations. For this, the NP dispersions were serially diluted twofold with sterile water. Double-concentrated DMEM (20% FBS, supplemented with the corresponding amount of sodium bicarbonate (#S5761, Sigma-Aldrich, St. Louis, MO)), prepared and filter-sterilized from DMEM powder (#12800082, Thermo Fisher Scientific, Waltham, MA), was added to each well in the ratio of 1:1 (water solution of the sample:double-concentrated DMEM). After 24 h of incubation, the medium was replaced with a resazurin-containing complete medium (15 μg/mL, #R7017, Sigma-Aldrich), and the plates were incubated for 3−4 h in a humidified atmosphere containing 5% CO_2 at 37 °C. Absorbance intensity (570 nm) was then measured using a Cytation 5 Imaging Reader (Biotek, Winooski, VT).

Flow Cytometry. For the NR-labeled NP uptake study, the cells were seeded at a density of 250 000 cells per well in a 12-well plate (in 2 mL of the media). The next day, the NPs were added at a final concentration of 17 μg/mL at the desired time points. After washing with prewarmed BSA solution (1% in PBS, #P3688, Sigma-Aldrich), the cells were harvested by scraping or trypsin treatment, as appropriate, and resuspended in 1 mL of BSA solution. The samples were analyzed by flow cytometry (CytoFLEX, Beckman Coulter, Brea, CA), using a 488 nm laser to excite the fluorescence of NR. Cells were analyzed at the rate of ∼200 events/s and data (50 000 total events per sample) were analyzed using CytExpert Software (Beckman Coulter); the mean cell-associated fluorescence was determined in the PE channel. For the analysis, only a live cell population was considered in terms of gating. For this purpose, an assay based on propidium iodide (#P4170, Sigma-Aldrich) and calcein-AM (part of the LIVE/DEAD Viability/Cytotoxicity Kit, #L3224, Thermo Fisher Scientific) was used (data not shown).

For data representation, mean fluorescence intensity values were normalized to a nontreated control group. Next, using GraphPad Prism software (Dotmatics, Boston, MA), internalization half-time values were calculated based on the internalization time course by curve-fitting of the data using the following equation

$$F(t) = F_0 + (F_{\text{plateau}} - F_0)(1 - e^{-tk}) \quad (1)$$

where $F(t)$ is the cell fluorescence signal at time t, F_0 and F_{plateau} are the initial fluorescence signal and the maximum signal, respectively, and k is the internalization rate constant. The half-time of internalization was calculated as the ratio of ln 2 and k.[40,48]

Microscopic Analysis. Both J774A.1 and MCF-7 cells were seeded at the bottom of 8-well glass-bottomed chambers (#C8-1.5H-N, Cellvis, Mountain View, CA) at a density of 50 000 cells/well and left to adhere overnight. Next, at the desired time points, the medium was replaced with DMEM containing the NR-labeled PLGA NPs at 17 μg/mL. The cells were washed using PBS and then fixed (prechilled 4% paraformaldehyde in PBS, 10 min), followed by counterstaining with 4′,6-diamidino-2-phenylindole (DAPI, 300 nM in PBS, 10 min), and 3 washing steps (PBS). The cells were immersed in a Fluoromount-G mounting medium (Thermo Fisher Scientific). Visualization of monocytes-macrophages was carried out using a Zeiss LSM 880 microscope (Zeiss, Oberkochen, Germany) with a 63× oil objective (Objective Plan-Apochromat 63×/1.4 Oil DIC M27). Signal detection (pinholes 80 μm) was observed at channels Ch 1 (excitation 405 nm, emission 415−473 nm, DAPI) and Ch 2 (excitation 552 nm, emission 579−636 nm). Similarly, NPs' cellular uptake by MCF-7 cells was analyzed using a BioTek Lionheart FX Automated Microscope for both DAPI and Rh-B (excitation 560 nm, emission 583 nm) field.

Drug Encapsulation, Therapeutic Studies, and Analytical Methods. A nanoprecipitation method was used to encapsulate doxorubicin (DOX) into the core of the PLGA NP. In a typical encapsulation process, different amounts of DOX (25, 50, 100, 150, and 200 μg per mg of PLGA) solution in dimethyl sulfoxide (DMSO) were mixed with 1 mg of PLGA dissolved in acetonitrile. Following the NP preparation protocol (as detailed in the Nanoparticle Preparation section), the entire mixture in 400 μL was added dropwise to the aqueous solution of DSPE-PEG-COOH, which resulted in the self-assembly of NPs that encapsulate DOX in its core. During this nanoprecipitation process, the temperature of the aqueous container was maintained at 60 °C. After the formation of DOX-loaded NPs, the content was purified using an Amicon filter with a molecular-weight cut-off of 100 kDa. This allows us to remove any free-floating drug, lipid, or polymer as all of these materials are less than 50 kDa, and the NP prepared was more than 60 nm, which stays unfiltered and can be recovered easily in the media of interest, herein phosphate-buffered saline (PBS). Drug-encapsulated NP (DOX-NP) was characterized using multiangle dynamic light scattering (MADLS) for their colloidal and electrical properties. Drug-loaded NPs after purification were lyophilized (Labonco freezone) and the total dry weight of the drug-loaded NPs was recorded. A dry powder of drug-loaded NPs was dissolved in an acetonitrile:water (80:20 volume ratio) mixture to dissolve the PLGA. After filtration through a 200 nm filter, drug loading was quantified spectrophotometrically at 490 nm following the DOX calibration plot.

With the success in DOX loading, we moved forward to study the therapeutic potential of these NPs against human breast cancer MCF-7 cells in terms of percentage cell viability following Cell Counting Kit-8 (CCK-8, GLPBIO, catalog#GK10001, (2-(2-methoxy-4-nitrophenyl)-3-(4-nitrophenyl)-5-(2,4-disulfophenyl)-2H-tetrazolium, monosodium salt)) assay. Briefly, 10 000 cells were seeded in 96-well plates. After 24 h, DOX-NP and free DOX were added to the cells at varying DOX concentrations. Cells were treated for 24 and 48 h in a 5% CO_2 environment at 37 °C. After each time point, the cells were washed with PBS and incubated with Cell Counting Kit-8, which is a water-soluble tetrazolium salt that produces the water-soluble formazan dye, for 4 h. The principle behind this assay is that the live cells will react with the CCK-8 reagent to form soluble formazan. The absorbance of the solution was measured at 450 nm using a microplate reader (BioTek, Synergy H1 Hybrid Reader) to calculate the percentage cell viability. Each treatment was repeated in three different experiments in 96-well plates (n = 3). In every 96-well plate, 6 wells were used for a single concentration type to obtain robust data. The half-maximal inhibitory concentration (IC_{50}) was quantified using GraphPad

https://doi.org/10.1021/acsomega.3c02273
ACS Omega 2023, 8, 27146−27155

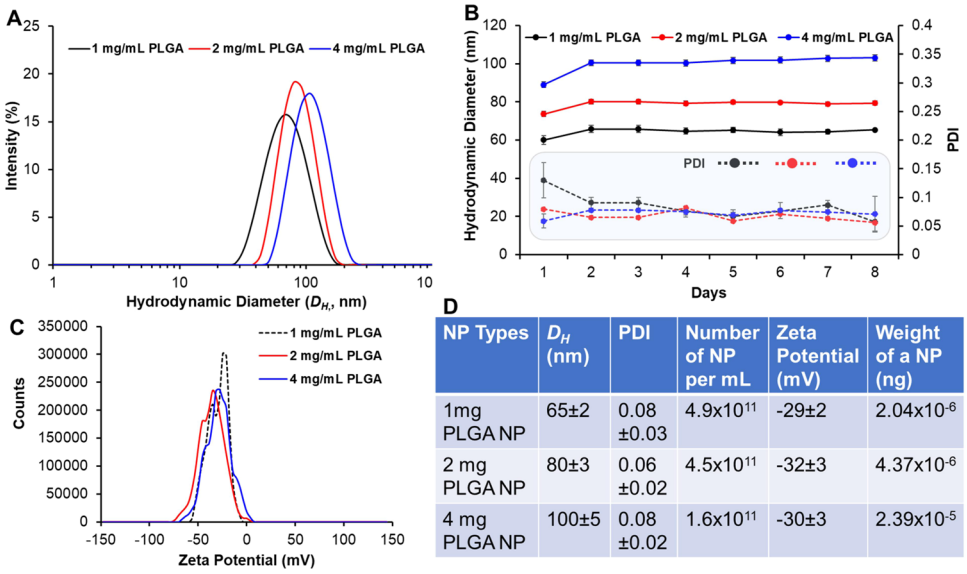

D

NP Types	D_H (nm)	PDI	Number of NP per mL	Zeta Potential (mV)	Weight of a NP (ng)
1mg PLGA NP	65±2	0.08 ±0.03	4.9×10^{11}	-29±2	2.04×10^{-6}
2 mg PLGA NP	80±3	0.06 ±0.02	4.5×10^{11}	-32±3	4.37×10^{-6}
4 mg PLGA NP	100±5	0.08 ±0.02	1.6×10^{11}	-30±3	2.39×10^{-5}

Figure 1. Physiochemical characterization of PLGA nanoparticles. (A) Dynamic light scattering measurement showing the hydrodynamic size of three different types of NPs. (B) Colloidal stability of NPs determined by measuring the hydrodynamic size and polydispersity index (PDI) over the period. (C) ζ-potential of the respective NPs. (D) Table showing a summary of the colloidal properties of the NPs, in which the number of NPs was determined using multiangle dynamic light scattering (MADLS) and the weight of the NPs was determined by accounting gravimetric weight using the number of NPs. All of these experiments were conducted at 1 mg/mL NP concentration in an aqueous solution. Data represent mean ± SD, $n = 3$.

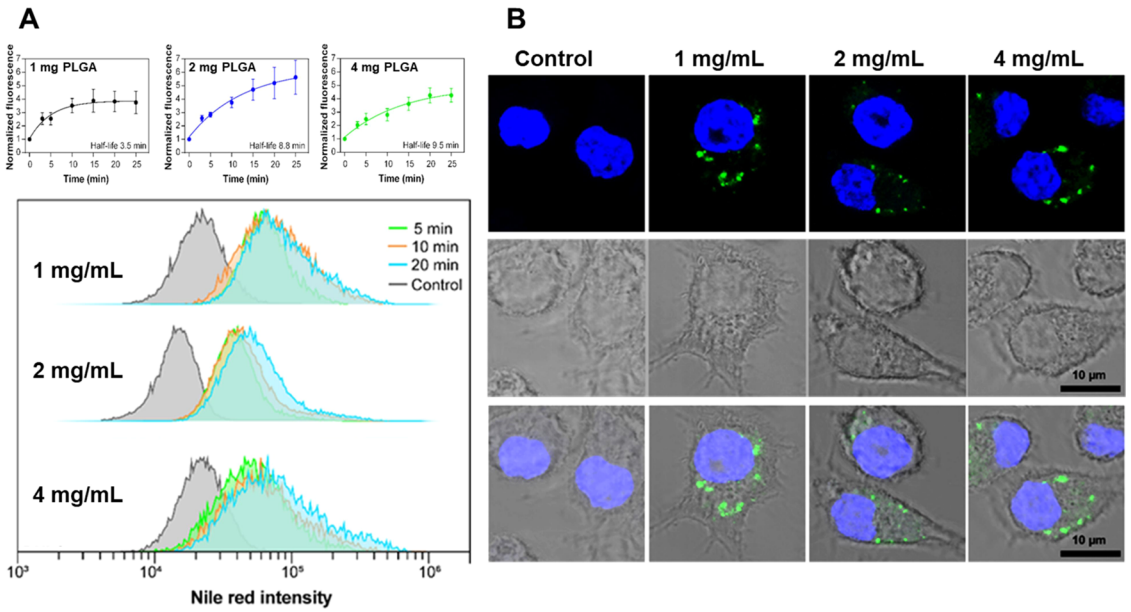

Figure 2. NP cell uptake study in an immune cell. The cells were incubated with NR-labeled NPs at 17 μg/mL and the time courses of NP uptake by J774A.1 monocyte-macrophages were assessed using flow cytometry (A). The normalized cell-associated fluorescence increase was fitted using a mono-exponential function to calculate the association half-time values. Flow cytometry result comparison as the mean cell-associated fluorescence intensity. Images from confocal laser scanning microscopy (B) of J774A.1 cell after 20 min of incubation with different NP types at 17 μg/mL. LissRh-labeled NPs (pseudo green color) were used; DAPI (blue) was used to visualize the cell nuclei. Data represent ± SD, $n = 3$.

software following the "dose response-inhibition" model. For cellular DOX quantification, high-performance liquid chromatography (Waters e2695 HPLC system equipped with symmetry C18 Column, 100Å, 5 μm, 4.6 mm × 150 mm) was used. For this purpose, cells in T-25 flask were treated with free DOX ($n = 3$) and DOX-NP ($n = 3$) for 30 min, and the cells were washed and collected via trypsinization. The collected cells' number was counted using a Bio-Rad TC20 automated cell counter and the cells were lysed in water containing a 0.05% trifluoracetic acid and acetonitrile mixture (50:50 volume ratio). Lysed cells were centrifuged to remove any debris, filtered through a 200 nm polytetrafluoroethylene polymer (PTFE) filter, and injected into the HPCL system consisting of Waters 2489-UV/Vis-detector. The mobile phase was water:acetonitrile (80:20 volume ratio); an isocratic elution was programmed for 10 min at a flow rate of 300 μL/min (DOX retention time = 3.9 min, $\lambda = 230$ nm).

https://doi.org/10.1021/acsomega.3c02273
ACS Omega 2023, 8, 27146−27155

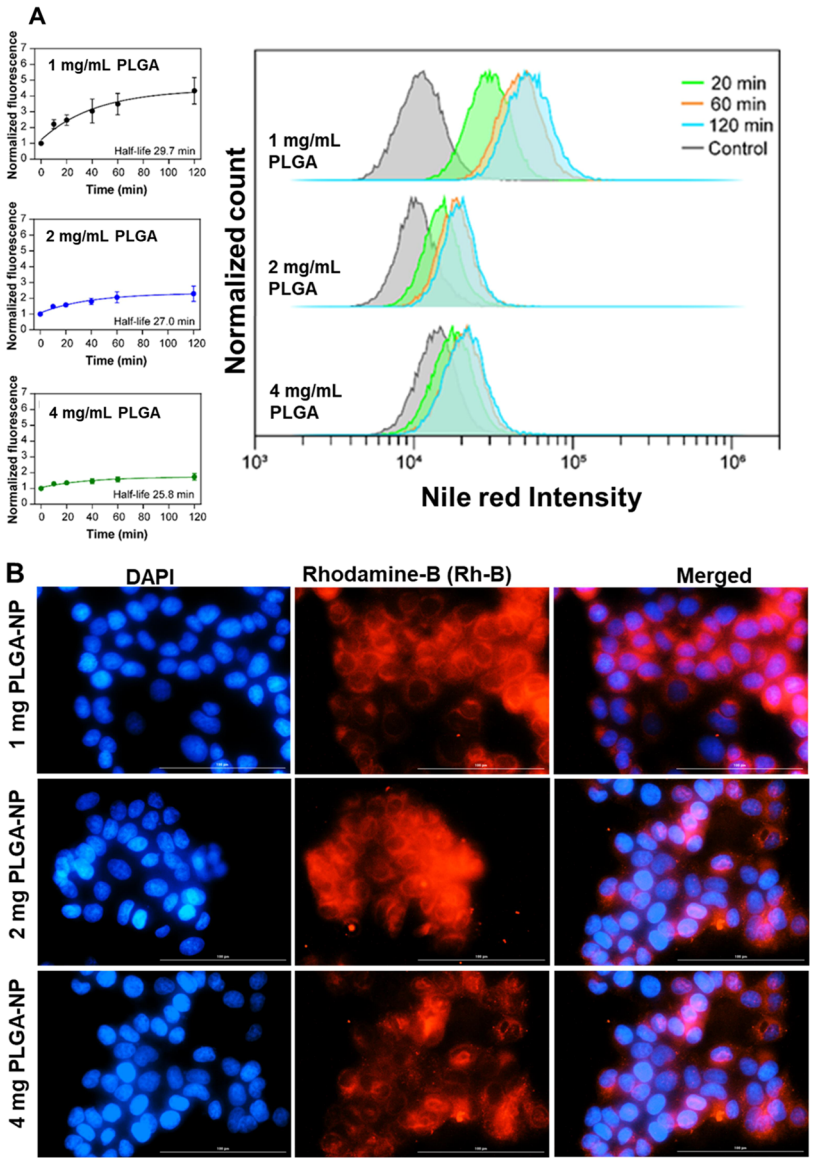

Figure 3. NP cell uptake study in a cancer cell. The cells were incubated with NR-labeled NPs at 17 μg/mL and the time courses of NP uptake by MCF-7 breast cancer cells were assessed using flow cytometry (A). The normalized cell-associated fluorescence increase was fitted using a mono-exponential function to calculate the association half-time values. Flow cytometry result comparison with the mean cell-associated fluorescence intensity. Lionheart FX Automated Microscope images (B) of MCF-7 cells after 20 min of incubation with different NP types at 17 μg/mL. LissRh-labeled NPs were used; DAPI (blue) was used to visualize the cell nuclei. Scale bar 100 μm. Data represent ± SD, $n = 3$.

RESULTS AND DISCUSSION

Synthesis and Characterization of PLGA NPs. PLGA NPs of varying weights were synthesized following nanoprecipitation while keeping the solvent ratio constant in all preparations. In nanoprecipitation, the contents in two miscible solvents, which otherwise are not soluble in the same solvent, were mixed for self-assembly. In this way, PLGA NPs were finally obtained in a total volume of 4 mL containing 2.6 mL of 4% ethanol and 400 μL of acetonitrile at 65 °C. The use of 4% ethanol facilitates the solubility of DSPE-PEG-COOH and precipitation of PLGA; therefore, this combination initiates self-assembly efficiently when hydrophobic PLGA comes in contact. Finally, 1 mL of water was added to the mixture to quench the temperature. Most importantly, in all preparations, varying concentrations of PLGA (1, 2, and 4 mg) in acetonitrile were nanoprecipitated in a confined constant volume of precipitant containing the stabilizer DSPE-PEG-COOH; this leads to an increase in the resulting weight of NP while increasing the concentration of PLGA (Figure 1A–D). Moreover, the organic solvents (i.e., acetonitrile and ethanol) used in our study are all miscible in water; the solvent in the organic phase migrates spontaneously toward the water phase once the polymer solution in the organic solvent is introduced into water. Such a quick change of the solvent composition around the polymer molecules decreases the interfacial tension between the aqueous and organic phases, resulting in rapid diffusion and finally inducing solidification of the polymer (i.e., precipitation by crystallization or vitrification), and subsequently NP formation.[49] During this process, the diffusion rate is expected to be governed largely by the polymer–solvent (acetonitrile), polymer–nonsolvent (water and alcohol), and solvent–nonsolvent interaction as well as the viscosity of the polymer solution. MADLS showed that these particles are unimodal in size, ranging from 65 to 100 nm with a narrow

https://doi.org/10.1021/acsomega.3c02273
ACS Omega 2023, 8, 27146–27155

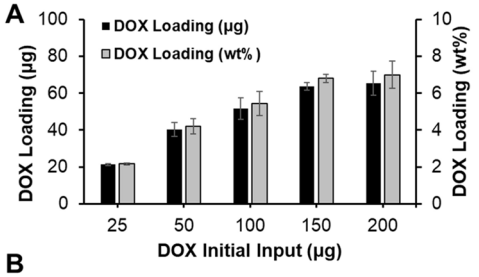

DOX Initial Input (μg/mg PLGA)	DOX-NP D_H (nm)	Polydispersity Index (PDI)	Zeta Potential (mV)
25	68±3	0.21±0.02	-32±3
50	70±3	0.19±0.01	-31±2
100	75±5	0.12±0.02	-32±3
150	77±5	0.22±0.03	-34±4
200	80±9	0.25±0.02	-36±6

Figure 4. Drug loading studies. (A) Comparative DOX loading efficiency of PLGA NPs with various initial input feeding concentrations of DOX (25−200 μg). (B) Colloidal properties of DOX-loaded PLGA NPs (DOX-PLGA). Data represent mean ± SD, n = 3.

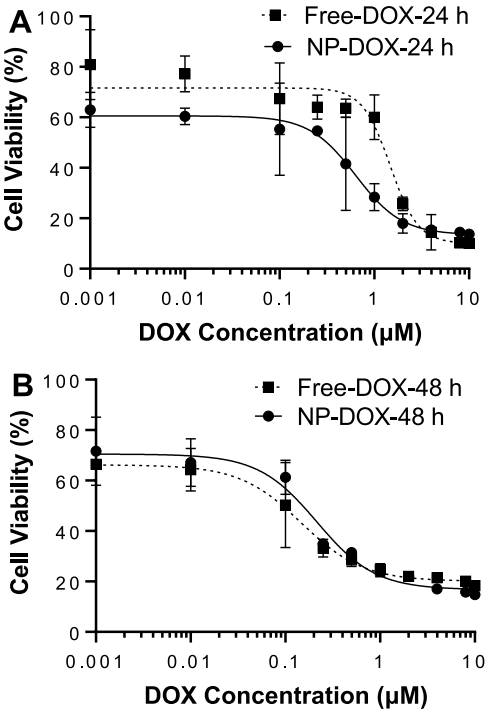

Figure 5. Therapeutic study against human breast cancer MCF-7 cells. The comparative cytotoxicity of free DOX and DOX-PLGA NPs against MCF-7 cells (A) 24 h and (B) 48 h post-treatment was studied using CCK-8 assay. Data represent mean ± SD, n = 3.

polydispersity of < 0.2 (Figure 1A). We further evaluated the stability of NPs at room temperature for a period of 8 days (Figure 1B). The observation from the stability studies depicted that these NPs are highly stable in an aqueous solution and there is no significant change in their size and PDI from day 1 to day 8. These particles are surface passivated with carboxylate-terminated poly(ethylene glycol), resulting in a negative ζ-potential. Most importantly, there is no significant change in ζ-potential, which further assured us that all formulations are well structured with nearly similar surface property. This will give us robust environments to understand cellular uptake due to the weight and size of the NPs as the chemistry of the particles is the same due to the use of the same component that varies only in the amount of core PLGA. However, we observed a decrease in NP concentration with the increase in weight of the NP, which further confirmed the packing of the PLGA polymer during nanoprecipitation at the core, thereby increasing the size and weight (Figure 1A−D).

Evaluation of the Cytotoxicity of NPs. For any biomedical application, toxicological analysis of NPs is a highly recommended observation before any other biological analysis. In the body, highly active immune cells such as macrophages recognize these NPs as a foreign body and immediately act on them to scavenge these foreign materials as a first step in the body's defense mechanism. Therefore, we selected monocyte-macrophages J774.1A and human breast cancer cell MCF-7 for NPs' cytocompatibility evaluation using resazurin cell viability assay. The resazurin assay detects the chemical reduction of growth medium resulting from cell growth as an indicator of cell viability, proliferation, and cytotoxicity, in which we look for the redox indicator to change from the oxidized form (nonfluorescent, blue) to the reduced form (fluorescent resorufin, pink). To analyze the possible alteration in metabolic activity due to all types of NPs presented herein, we analyzed the NP cytotoxicity at varying NP concentrations and incubation times (Figure S1). We observed no significant reduction in cellular activity; all NP types maintain more than 95% cell viability, showing that these NPs are compatible with both cell types, and therefore, are ready for further cellular studies.

Cellular Uptake Studies. The goal of this study is to evaluate the influence of NPs' weight on cellular uptake kinetics. Cell surface chemistry is unique to respective cell types, which in turn govern NPs' uptake. Among the cells, immune cells such as macrophages are designed to phagocytose foreign materials and play an important role in eliminating diseased and damaged cells through their programmed cell death. Typically, this process involves various phases, which include the detection of particles, activation of the internalization process, and formation of the phagosome and its maturation.[50,51] As expected, we observed a rapid uptake of these NPs by monocyte-macrophages as compared to cancer cells. The half-time of the uptake kinetics for lighter NPs was lesser than that of heavier particles in both cell types. For monocyte-macrophages, we found that half of the NPs treated were cell-associated within 3.5 min (Figure 2), whereas the cancer cell uptake kinetics ranges from 25 to 30 min (Figure 3). Data show that cancer cells internalize NPs slower than monocyte-macrophages. In the tested NP ranges, cancer cells sequestrated denser particles (4 mg/mL PLGA) slightly faster (half-time = 25.8 min, Figure 3) than less dense particles (half-time = 29.7 min, Figure 2). In contrast, macrophages uptake lighter NPs faster (3.5 min, Figure 2) than heavier NPs (9.5 min, Figure 2). Cellular uptakes were further supported by microscopic analysis, which was conducted at constant NP concentrations in both cell types, and the observation showed that lighter NPs are uptaken more efficiently. Overall, the results highlight the role of NP weight in cellular uptake. A confocal laser scanning microscope (CLSM) and BioTek Lionheart FX Automated microscope were used to assess NPs' interaction with monocyte-macrophages and cancer cells,

https://doi.org/10.1021/acsomega.3c02273
ACS Omega 2023, 8, 27146−27155

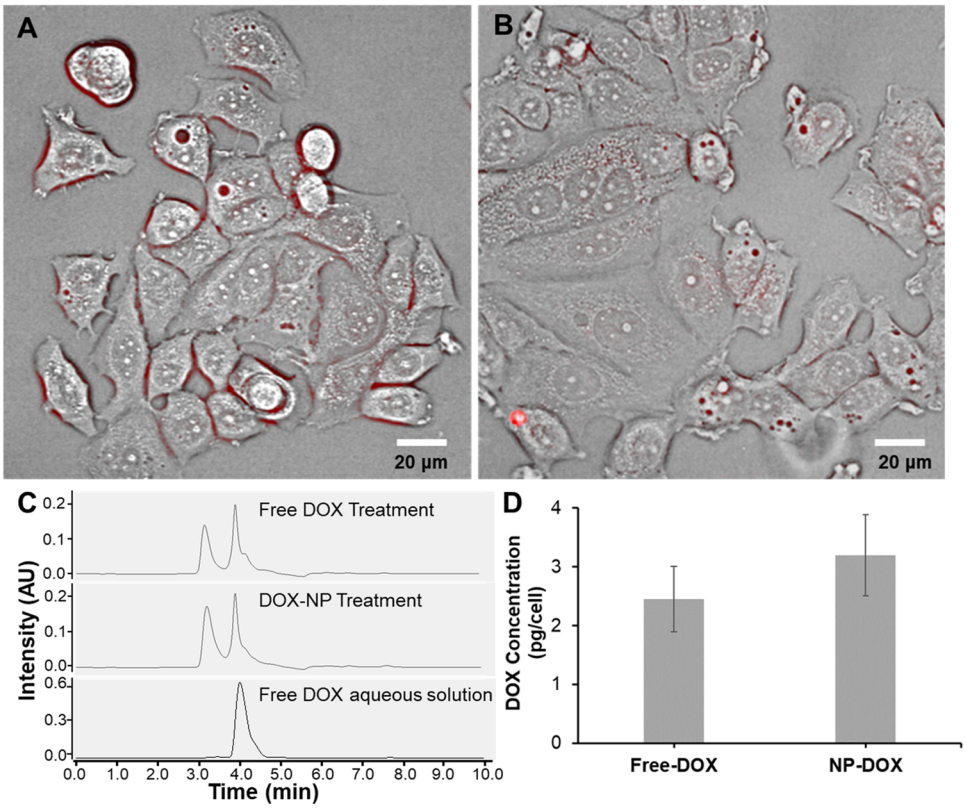

Figure 6. Cellular quantification of doxorubicin. (A) Cells treated with free DOX. (B) Cells treated with DOX-NP. (C) A representative HPLC chromatogram of an aqueous solution of DOX, free DOX-, and DOX-NP-treated cells. (D) Quantification of DOX in free-DOX and DOX-NP-treated groups. Data represent mean ± SD, n = 3.

respectively, by reading the Rh-B fluorescence. It was found that all of the NP samples fabricated are sequestrated by both cell types, namely J774A.1 monocyte-macrophages and human breast cancer MCF-7 cells. Considering the widespread use of NP-based delivery systems due to several advantages including prolonged delivery times, targeting of drugs to specialized cells, and cytocompatibility, we hope this will pave a small step in drug delivery technology development.

Anticancer Efficiency. With the confirmation of the cytocompatibility and cellular internalization kinetics, we further moved forward to understand the therapeutic potential of the fabricated NPs. Considering the faster kinetics and stability of the synthesized NPs, we chose the NP made up of 1 mg of PLGA (sample 1 mg/mL PLGA) as the candidate NP for anticancer drug delivery. For this purpose, anticancer doxorubicin (DOX) was chosen as the model drug following the US FDA's recommendation for breast cancer treatment.[52,53] Drug loading content was evaluated using the sequential initial input of DOX from 25 μg/mg PLGA to 200 μg/mg PLGA (Figure 4A).

The results showed an overall increase in the drug loading content from 20 μg/mg PLGA to 70 μg/mg PLGA (Figure 4A). DOX is regarded as a cationic drug at pH 4−6 and carboxylate-terminated PLGA is negatively charged; therefore, DOX is preferentially entrapped into the PLGA core.[54] Entrapment of DOX into the core was further supported by the ζ-potential (Figure 4B), which is nearly equivalent to bare PLGA NPs, which otherwise would have exhibited a positive change in ζ-potential if the DOX were on the surface of PLGA NPs. While all of the resulting DOX-NPs were found to be stable (Figure 4B), we used DOX 100 μg/mg PLGA input due to its narrow PDI of 0.12 ± 0.02. DOX-loaded PLGA NPs were used to treat MCF-7 cells and cell viability was measured using the CCK-8 kit assay at 24 and 48 h of drug treatment. Using GraphPad Prism, the IC_{50} of the DOX-NPs was calculated as shown in Figure 5A,B. The IC_{50} of free DOX was recorded as 1.47 and 0.161 μM for variable drug treatment times of 24 and 48 h, respectively, whereas the IC_{50} of DOX-NPs shows the rapid killing of cancer cells with values of 0.636 and 0.214 μM when treated for 24 and 48 h, respectively (Figure 5B).

Therapeutic data show that DOX-NPs are highly potent than free DOX in the early hours. To understand this at a cellular level, we treated cells with free DOX and DOX-NP for 30 min as guided by FACS studies (Figure 6A−D) to quantify the cellular DOX level. After 30 min, the cells were washed, imaged, and the DOX associated with the cells was quantified using HPLC. Interesting cellular features were observed, in which the cellular boundaries appeared red due to DOX fluorescence in most of the cases with free-DOX-treated cells (Figure 6A), whereas in the case of DOX-NP-treated cells, the micrographs showed that DOX fluorescence is highly associated with vesicular structures, suggesting intracellular entrapment of the DOX-NPs (Figure 6B) and efficient trafficking of the studied intervention. To further understand the cellular concentration of DOX, we collected the cells and quantified DOX concentration using HPLC (Figure 6C,D). Figure 6C shows representative chromatograms of the respective groups containing an aqueous solution of DOX, free-DOX-treated cancer cells, and DOX-NP-treated cancer cells. A quantitative evaluation of DOX isolated from cancer cells is presented in Figure 6D, which showed that a detectable

https://doi.org/10.1021/acsomega.3c02273
ACS Omega 2023, 8, 27146−27155

amount of DOX is associated with cells in which a higher amount of DOX was isolated from DOX-NP-treated cancer cells. These quantitative data also support our evidence of rapid cancer inhibition in the early hours (Figure 5A). The phenomenon is probably related to the fast internalization kinetics of NP drug that increases the local drug concentration in the cell. As discussed in the literature,[55−61] the higher potency of DOX-NP can be explained by acknowledging the various endocytic pathways that the NP system acquires due to its higher surface area and possible PEG shedding to expose the phospholipid to fuse with the endosome membrane to release the maximum drug into the cytosol for therapeutic effect. To further confirm this phenomenon as reported in the literature, further studies are warranted that demand modifying the surface of the NP with receptor-targeting ligands, multiple receptor blocking, and detailed microscopic experiments.

CONCLUSIONS

NPs interact with our body in many different ways, but their deleterious effects primarily arise from interaction at cellular and subcellular levels. These interactions are governed by many different mechanisms, including receptor-mediated endocytosis, diffusion, and direct penetration, where the cell surface protein and surface chemistry of the NPs play a significant role. These processes are more prominent when NPs are in proximity to the cell surface, which we have seen in our observation and is found to be cell-specific. The results showed that lighter NPs are uptaken faster with an internalization half-time of 3.5 min compared to the heavier NPs with an internalization half-time of 9.5 min, which is cell-specific, with monocyte-macrophages being uptaken faster than cancer cells. These NPs efficiently deliver DOX into the cell showing concentration-dependent cytotoxicity against breast cancer cells, as observed from the HPLC results. The surface properties of all NP types in this experiment were maintained nearly constant, which further supports the influence of NP weight on the cellular uptake, while further study is warranted to envision the receptor status and possible endocytic mechanism. We are optimistic that this fundamental study will pave the path for consideration of the weight of NPs in the study design of drug delivery applications.

ASSOCIATED CONTENT

Supporting Information

The Supporting Information is available free of charge at https://pubs.acs.org/doi/10.1021/acsomega.3c02273.

Dose-dependent cytocompatibility of all types of NPs against cancer (MCF-7) and immune (J774A.1) cells (PDF)

AUTHOR INFORMATION

Corresponding Author

Santosh Aryal − *Department of Pharmaceutical Sciences and Health Outcomes, The Ben and Maytee Fisch College of Pharmacy, The University of Texas at Tyler, Tyler, Texas 75799, United States;* orcid.org/0000-0002-7807-6342; Email: santosharyal@uttyler.edu

Authors

Prabhat Kattel − *Department of Pharmaceutical Sciences and Health Outcomes, The Ben and Maytee Fisch College of Pharmacy, The University of Texas at Tyler, Tyler, Texas 75799, United States*

Shoukath Sulthana − *Department of Pharmaceutical Sciences and Health Outcomes, The Ben and Maytee Fisch College of Pharmacy, The University of Texas at Tyler, Tyler, Texas 75799, United States*

Jiří Trousil − *Department of Pharmaceutical Sciences and Health Outcomes, The Ben and Maytee Fisch College of Pharmacy, The University of Texas at Tyler, Tyler, Texas 75799, United States; Institute of Macromolecular Chemistry, Czech Academy of Sciences, Prague 16200, Czech Republic*

Dinesh Shrestha − *Department of Pharmaceutical Sciences and Health Outcomes, The Ben and Maytee Fisch College of Pharmacy, The University of Texas at Tyler, Tyler, Texas 75799, United States*

David Pearson − *Department of Pharmaceutical Sciences and Health Outcomes, The Ben and Maytee Fisch College of Pharmacy, The University of Texas at Tyler, Tyler, Texas 75799, United States*

Complete contact information is available at: https://pubs.acs.org/10.1021/acsomega.3c02273

Author Contributions

§P.K. and S.S. contributed equally.

Notes

The authors declare no competing financial interest.

ACKNOWLEDGMENTS

The authors thank the support from the National Institute of Biomedical Imaging and Bioengineering, National Institute of Health under Grant No. 7R15EB030815-02. J.T. thanks the financial support from the Czech Academy of Sciences (Project No. MSM200502101) and acknowledges UT-Tyler for research training and advancement opportunity. The authors also thank the support from the University of Texas System Rising STARs award and the open access article publishing partial support from the University of Texas at Tyler.

REFERENCES

(1) Park, J.; Fong, P. M.; Lu, J.; Russell, K. S.; Booth, C. J.; Saltzman, W. M.; Fahmy, T. M. PEGylated PLGA Nanoparticles for the Improved Delivery of Doxorubicin. *Nanomed. Nanotechnol. Biol. Med.* **2009**, *5*, 410−418.

(2) Nguyen, T. D. T.; Pitchaimani, A.; Bahadur Koirala, M.; Muhammad, F.; Aryal, S. Engineered Biomimetic Nanoabsorbent for Cellular Detoxification of Chemotherapeutics. *RSC Adv.* **2016**, *6*, 33003−33008.

(3) Swami, A.; Reagan, M. R.; Basto, P.; Mishima, Y.; Kamaly, N.; Glavey, S.; Zhang, S.; Moschetta, M.; Seevaratnam, D.; Zhang, Y.; Liu, J.; Memarzadeh, M.; Wu, J.; Manier, S.; Shi, J.; Bertrand, N.; Lu, Z. N.; Nagano, K.; Baron, R.; Sacco, A.; Roccaro, A. M.; Farokhzad, O. C.; Ghobrial, I. M. Engineered Nanomedicine for Myeloma and Bone Microenvironment Targeting. *Proc. Natl. Acad. Sci. U.S.A.* **2014**, *111*, 10287−10292.

(4) Hu, C.-M. J.; Fang, R. H.; Copp, J.; Luk, B. T.; Zhang, L. A Biomimetic Nanosponge That Absorbs Pore-Forming Toxins. *Nat. Nanotechnol.* **2013**, *8*, 336−340.

(5) Aryal, S.; Hu, C.-M. J.; Fang, R. H.; Dehaini, D.; Carpenter, C.; Zhang, D.-E.; Zhang, L. Erythrocyte Membrane-Cloaked Polymeric Nanoparticles for Controlled Drug Loading and Release. *Nanomedicine* **2013**, *8*, 1271−1280.

(6) Aryal, S.; Hu, C.-M. J.; Zhang, L. Polymer−Cisplatin Conjugate Nanoparticles for Acid-Responsive Drug Delivery. *ACS Nano* **2010**, *4*, 251−258.

(7) Aryal, S.; Stigliano, C.; Key, J.; Ramirez, M.; Anderson, J.; Karmonik, C.; Fung, S.; Decuzzi, P. Paramagnetic Gd(3+) Labeled Red Blood Cells for Magnetic Resonance Angiography. *Biomaterials* **2016**, *98*, 163−170.
(8) Nguyen, T. D. T.; Pitchaimani, A.; Aryal, S. Engineered Nanomedicine with Alendronic Acid Corona Improves Targeting to Osteosarcoma. *Sci. Rep.* **2016**, *6*, No. 36707.
(9) Ferrari, M. Cancer Nanotechnology: Opportunities and Challenges. *Nat. Rev. Cancer* **2005**, *5*, 161−171.
(10) Chen, H.; Shao, L.; Li, Q.; Wang, J. Gold Nanorods and Their Plasmonic Properties. *Chem. Soc. Rev.* **2013**, *42*, 2679−2724.
(11) Arvizo, R.; Bhattacharya, R.; Mukherjee, P. Gold Nanoparticles: Opportunities and Challenges in Nanomedicine. *Expert Opin. Drug Delivery* **2010**, *7*, 753−763.
(12) Farokhzad, O. C.; Langer, R. Impact of Nanotechnology on Drug Delivery. *ACS Nano* **2009**, *3*, 16−20.
(13) Behzadi, S.; Serpooshan, V.; Tao, W.; Hamaly, M. A.; Alkawareek, M. Y.; Dreaden, E. C.; Brown, D.; Alkilany, A. M.; Farokhzad, O. C.; Mahmoudi, M. Cellular Uptake of Nanoparticles: Journey Inside the Cell. *Chem. Soc. Rev.* **2017**, *46*, 4218−4244.
(14) Sakamoto, J. H.; van de Ven, A. L.; Godin, B.; Blanco, E.; Serda, R. E.; Grattoni, A.; Ziemys, A.; Bouamrani, A.; Hu, T.; Ranganathan, S. I.; De Rosa, E.; Martinez, J. O.; Smid, C. A.; Buchanan, R. M.; Lee, S.-Y.; Srinivasan, S.; Landry, M.; Meyn, A.; Tasciotti, E.; Liu, X.; Decuzzi, P.; Ferrari, M. Enabling Individualized Therapy through Nanotechnology. *Pharmacol. Res.* **2010**, *62*, 57−89.
(15) Caron, W. P.; Morgan, K. P.; Zamboni, B. A.; Zamboni, W. C. A Review of Study Designs and Outcomes of Phase I Clinical Studies of Nanoparticle Agents Compared with Small-Molecule Anticancer Agents. *Clin. Cancer Res.* **2013**, *19*, 3309−3315.
(16) Muhammad, F.; Nguyen, T. D. T.; Raza, A.; Akhtar, B.; Aryal, S. A Review on Nanoparticle-Based Technologies for Biodetoxification. *Drug Chem. Toxicol.* **2017**, *40*, 489−497.
(17) Akter, M.; Sikder, M. T.; Rahman, M. M.; Ullah, A. K. M. A.; Hossain, K. F. B.; Banik, S.; Hosokawa, T.; Saito, T.; Kurasaki, M. A Systematic Review on Silver Nanoparticles-Induced Cytotoxicity: Physicochemical Properties and Perspectives. *J. Adv. Res.* **2018**, *9*, 1−16.
(18) Wilhelm, S.; Tavares, A. J.; Dai, Q.; Ohta, S.; Audet, J.; Dvorak, H. F.; Chan, W. C. W. Analysis of Nanoparticle Delivery to Tumours. *Nat. Rev. Mater.* **2016**, *1*, 16014.
(19) Shi, J.; Kantoff, P. W.; Wooster, R.; Farokhzad, O. C. Cancer Nanomedicine: Progress, Challenges and Opportunities. *Nat. Rev. Cancer* **2017**, *17*, 20−37.
(20) Kabanov, A. V.; Gendelman, H. E. Nanomedicine in the Diagnosis and Therapy of Neurodegenerative Disorders. *Prog. Polym. Sci.* **2007**, *32*, 1054−1082.
(21) Chithrani, D. B. Nanoparticles for Improved Therapeutics and Imaging in Cancer Therapy. *Recent Pat. Nanotechnol.* **2010**, *4*, 171−180.
(22) Bala, I.; Hariharan, S.; Kumar, M. N. V. R. PLGA Nanoparticles in Drug Delivery: The State of the Art. *Crit. Rev. Ther. Drug Carrier Syst.* **2004**, *21*, 387−422.
(23) Danhier, F.; Ansorena, E.; Silva, J. M.; Coco, R.; Le Breton, A.; Préat, V. PLGA-Based Nanoparticles: An Overview of Biomedical Applications. *J. Controlled Release* **2012**, *161*, 505−522.
(24) FDA's Regulatory Science Program for Generic PLA/PLGA-Based Drug Products. http://www.americanpharmaceuticalreview.com/Featured-Articles/188841-FDA-s-Regulatory-Science-Program-for-Generic-PLA-PLGA-Based-Drug-Products/ (accessed June 15, 2016).
(25) Platel, A.; Carpentier, R.; Becart, E.; Mordacq, G.; Betbeder, D.; Nesslany, F. Influence of the Surface Charge of PLGA Nanoparticles on Their in Vitro Genotoxicity, Cytotoxicity, ROS Production and Endocytosis. *J. Appl. Toxicol.* **2016**, *36*, 434−444.
(26) Wu, J.; Zhang, J.; Deng, C.; Meng, F.; Cheng, R.; Zhong, Z. Robust, Responsive, and Targeted PLGA Anticancer Nanomedicines by Combination of Reductively Cleavable Surfactant and Covalent Hyaluronic Acid Coating. *ACS Appl. Mater. Interfaces* **2017**, *9*, 3985−3994.
(27) Marasini, R.; Thanh Nguyen, T. D.; Rayamajhi, S.; Aryal, S. Synthesis and Characterization of a Tumor-Seeking LyP-1 Peptide Integrated Lipid−Polymer Composite Nanoparticle. *Mater. Adv.* **2020**, *1*, 469−480.
(28) Situ, J.-Q.; Wang, X.-J.; Zhu, X.-L.; Xu, X.-L.; Kang, X.-Q.; Hu, J.-B.; Lu, C.-Y.; Ying, X.-Y.; Yu, R.-S.; You, J.; Du, Y.-Z. Multifunctional SPIO/DOX-Loaded A54 Homing Peptide Functionalized Dextran-g-PLGA Micelles for Tumor Therapy and MR Imaging. *Sci. Rep.* **2016**, *6*, No. 35910.
(29) Schleich, N.; Sibret, P.; Danhier, P.; Ucakar, B.; Laurent, S.; Muller, R. N.; Jérôme, C.; Gallez, B.; Préat, V.; Danhier, F. Dual Anticancer Drug/Superparamagnetic Iron Oxide-Loaded PLGA-Based Nanoparticles for Cancer Therapy and Magnetic Resonance Imaging. *Int. J. Pharm.* **2013**, *447*, 94−101.
(30) Nguyen, T. D. T.; Pitchaimani, A.; Ferrel, C.; Thakkar, R.; Aryal, S. Nano-Confinement-Driven Enhanced Magnetic Relaxivity of SPIONs for Targeted Tumor Bioimaging. *Nanoscale* **2018**, *10*, 284−294.
(31) Karfeld-Sulzer, L. S.; Waters, E. A.; Kohlmeir, E. K.; Kissler, H.; Zhang, X.; Kaufman, D. B.; Barron, A. E.; Meade, T. J. Protein Polymer MRI Contrast Agents: Longitudinal Analysis of Biomaterials in Vivo. *Magn. Reson. Med.* **2011**, *65*, 220−228.
(32) Zhang, Y.; García-Gabilondo, M.; Grayston, A.; J Feiner, I. V.; Anton-Sales, I.; A Loiola, R.; Llop, J.; Ramos-Cabrer, P.; Barba, I.; Garcia-Dorado, D.; Gosselet, F.; Rosell, A.; Roig, A. PLGA Protein Nanocarriers with Tailor-Made Fluorescence/MRI/PET Imaging Modalities. *Nanoscale* **2020**, *12*, 4988−5002.
(33) Aryal, S.; Key, J.; Stigliano, C.; Landis, M. D.; Lee, D. Y.; Decuzzi, P. Positron Emitting Magnetic Nanoconstructs for PET/MR Imaging. *Small* **2014**, *10*, 2688−2696.
(34) Aryal, S.; Key, J.; Stigliano, C.; Ananta, J. S.; Zhong, M.; Decuzzi, P. Engineered Magnetic Hybrid Nanoparticles with Enhanced Relaxivity for Tumor Imaging. *Biomaterials* **2013**, *34*, 7725−7732.
(35) Mitragotri, S.; Lahann, J. Physical Approaches to Biomaterial Design. *Nat. Mater.* **2009**, *8*, 15−23.
(36) Albanese, A.; Tang, P. S.; Chan, W. C. W. The Effect of Nanoparticle Size, Shape, and Surface Chemistry on Biological Systems. *Annu. Rev. Biomed. Eng.* **2012**, *14*, 1−16.
(37) Wang, J.; Byrne, J. D.; Napier, M. E.; DeSimone, J. M. More Effective Nanomedicines through Particle Design. *Small* **2011**, *7*, 1919−1931.
(38) Pitchaimani, A.; Nguyen, T. D. T.; Koirala, M.; Zhang, Y.; Aryal, S. Impact of Cell Adhesion and Migration on Nanoparticle Uptake and Cellular Toxicity. *Toxicol. In Vitro* **2017**, *43*, 29−39.
(39) Win, K. Y.; Feng, S.-S. Effects of Particle Size and Surface Coating on Cellular Uptake of Polymeric Nanoparticles for Oral Delivery of Anticancer Drugs. *Biomaterials* **2005**, *26*, 2713−2722.
(40) Urbánek, T.; Trousil, J.; Rak, D.; Gunár, K.; Konefał, R.; Šlouf, M.; Sedlák, M.; Šebestová Janoušková, O.; Hrubý, M. γ-Butyrolactone Copolymerization with the Well-Documented Polymer Drug Carrier Poly(Ethylene Oxide)-Block-Poly(ε-Caprolactone) to Fine-Tune Its Biorelevant Properties. *Macromol. Biosci.* **2020**, *20*, No. 1900408.
(41) Crucho, C. I. C.; Barros, M. T. Formulation of Functionalized PLGA Polymeric Nanoparticles for Targeted Drug Delivery. *Polymer* **2015**, *68*, 41−46.
(42) Eshete, M.; Bailey, K.; Nguyen, T. D. T.; Aryal, S.; Choi, S.-O. Interaction of Immune System Protein with PEGylated and Un-PEGylated Polymeric Nanoparticles. *Adv. Nanopart.* **2017**, *06*, 103.
(43) Fang, R. H.; Chen, K. N. H.; Aryal, S.; Hu, C.-M. J.; Zhang, K.; Zhang, L. Large-Scale Synthesis of Lipid−Polymer Hybrid Nanoparticles Using a Multi-Inlet Vortex Reactor. *Langmuir* **2012**, *28*, 13824−13829.
(44) Aryal, S.; Hu, C.-M. J.; Fu, V.; Zhang, L. Nanoparticle Drug Delivery Enhances the Cytotoxicity of Hydrophobic−Hydrophilic Drug Conjugates. *J. Mater. Chem.* **2012**, *22*, 994−999.

https://doi.org/10.1021/acsomega.3c02273
ACS Omega 2023, 8, 27146−27155

(45) Makadia, H. K.; Siegel, S. J. Poly Lactic-Co-Glycolic Acid (PLGA) as Biodegradable Controlled Drug Delivery Carrier. *Polymers* **2011**, *3*, 1377−1397.
(46) Schliecker, G.; Schmidt, C.; Fuchs, S.; Wombacher, R.; Kissel, T. Hydrolytic Degradation of Poly(Lactide-Co-Glycolide) Films: Effect of Oligomers on Degradation Rate and Crystallinity. *Int. J. Pharm.* **2003**, *266*, 39−49.
(47) Engineer, C.; Parikh, J.; Raval, A. Effect of Copolymer Ratio on Hydrolytic Degradation of Poly(Lactide-Co-Glycolide) from Drug Eluting Coronary Stents. *Chem. Eng. Res. Des.* **2011**, *89*, 328−334.
(48) Vainshtein, I.; Roskos, L. K.; Cheng, J.; Sleeman, M. A.; Wang, B.; Liang, M. Quantitative Measurement of the Target-Mediated Internalization Kinetics of Biopharmaceuticals. *Pharm. Res.* **2015**, *32*, 286−299.
(49) Krishnamoorthy, K.; Mahalingam, M. Selection of a Suitable Method for the Preparation of Polymeric Nanoparticles: Multi-Criteria Decision Making Approach. *Adv. Pharm. Bull.* **2015**, *5*, 57−67.
(50) Uribe-Querol, E.; Rosales, C. Phagocytosis: Our Current Understanding of a Universal Biological Process. *Front. Immunol.* **2020**, *11*, No. 1066.
(51) Lee, H.-J.; Woo, Y.; Hahn, T.-W.; Jung, Y. M.; Jung, Y.-J. Formation and Maturation of the Phagosome: A Key Mechanism in Innate Immunity against Intracellular Bacterial Infection. *Microorganisms* **2020**, *8*, 1298.
(52) Doxorubicin − FDA Prescribing Information, Side Effects and Uses. http://www.drugs.com/pro/doxorubicin.html.
(53) Tejada-Berges, T.; Granai, C. O.; Gordinier, M.; Gajewski, W. Caelyx/Doxil for the Treatment of Metastatic Ovarian and Breast Cancer. *Expert Rev. Anticancer Ther.* **2002**, *2*, 143−150.
(54) Tsai, L.-H.; Yen, C.-H.; Hsieh, H.-Y.; Young, T.-H. Doxorubicin Loaded PLGA Nanoparticle with Cationic/Anionic Polyelectrolyte Decoration: Characterization, and Its Therapeutic Potency. *Polymers* **2021**, *13*, 693.
(55) Mukherjee, S.; Kotcherlakota, R.; Haque, S.; Bhattacharya, D.; Kumar, J. M.; Chakravarty, S.; Patra, C. R. Improved Delivery of Doxorubicin Using Rationally Designed PEGylated Platinum Nanoparticles for the Treatment of Melanoma. *Mater. Sci. Eng. C* **2020**, *108*, No. 110375.
(56) Siegal, T.; Horowitz, A.; Gabizon, A. Doxorubicin Encapsulated in Sterically Stabilized Liposomes for the Treatment of a Brain Tumor Model: Biodistribution and Therapeutic Efficacy. *J. Neurosurg.* **1995**, *83*, 1029−1037.
(57) Tian, G.; Sun, X.; Bai, J.; Dong, J.; Zhang, B.; Gao, Z.; Wu, J. Doxorubicin-loaded Dual-functional Hyaluronic Acid Nanoparticles: Preparation, Characterization and Antitumor Efficacy in Vitro and in Vivo. *Mol. Med. Rep.* **2019**, *19*, 133−142.
(58) Clawson, C.; Ton, L.; Aryal, S.; Fu, V.; Esener, S.; Zhang, L. Synthesis and Characterization of Lipid−Polymer Hybrid Nanoparticles with PH-Triggered Poly (Ethylene Glycol) Shedding. *Langmuir* **2011**, *27*, 10556−10561.
(59) Trousil, J.; Filippov, S. K.; Hrubý, M.; Mazel, T.; Syrová, Z.; Cmarko, D.; Svidenská, S.; Matějková, J.; Kováčik, L.; Porsch, B.; Konefał, R.; Lund, R.; Nyström, B.; Raška, I.; Štěpánek, P. System with Embedded Drug Release and Nanoparticle Degradation Sensor Showing Efficient Rifampicin Delivery into Macrophages. *Nanomed. Nanotechnol. Biol. Med.* **2017**, *13*, 307−315.
(60) Trousil, J.; Syrová, Z.; Dal, N.-J. K.; Rak, D.; Konefał, R.; Pavlova, E.; Matějková, J.; Cmarko, D.; Kubíčková, P.; Pavliš, O.; Urbánek, T.; Sedlák, M.; Fenaroli, F.; Raška, I.; Štěpánek, P.; Hrubý, M. Rifampicin Nanoformulation Enhances Treatment of Tuberculosis in Zebrafish. *Biomacromolecules* **2019**, *20*, 1798−1815.
(61) Trousil, J.; Pavliš, O.; Kubíčková, P.; Škorič, M.; Marešová, V.; Pavlova, E.; Knudsen, K. D.; Dai, Y.-S.; Zimmerman, M.; Dartois, V.; Fang, J.-Y.; Hrubý, M. Antitubercular Nanocarrier Monotherapy: Study of In Vivo Efficacy and Pharmacokinetics for Rifampicin. *J. Controlled Release* **2020**, *321*, 312−323.

https://doi.org/10.1021/acsomega.3c02273
ACS Omega 2023, 8, 27146−27155